The Astrophysical Journal, 757:93 (8pp), 2012 September 20 doi:10.1088/0004-637X/757/1/93

PARTICLE ENERGY SPECTRA AT TRAVELING INTERPLANETARY SHOCK WAVES

Donald V. Reames
Institute for Physical Science and Technology, University of Maryland, College Park, MD 20742, USA; dvreames@umd.edu
Received 2012 May 5; accepted 2012 August 14; published 2012 September 6

ABSTRACT

We have searched for evidence of significant shock acceleration of He ions of ∼1–10 MeV amu^{-1} in situ at 258 interplanetary traveling shock waves observed by the *Wind* spacecraft. We find that the probability of observing significant acceleration, and the particle intensity observed, depends strongly upon the shock speed and less strongly upon the shock compression ratio. For most of the 39 fast shocks with significant acceleration, the observed spectral index agrees with either that calculated from the shock compression ratio or with the spectral index of the upstream background, when the latter spectrum is harder, as expected from diffusive shock theory. In many events the spectra are observed to roll downward at higher energies, as expected from Ellison–Ramaty and from Lee shock-acceleration theories. The dearth of acceleration at ∼85% of the shocks is explained by (1) a low shock speed, (2) a low shock compression ratio, and (3) a low value of the shock-normal angle with the magnetic field, which may cause the energy spectra that roll downward at energies below our observational threshold. Quasi-parallel shock waves are rarely able to produce measurable acceleration at 1 AU. The dependence of intensity on shock speed, seen here at local shocks, mirrors the dependence found previously for the peak intensities in large solar energetic-particle events upon speeds of the associated coronal mass ejections which drive the shocks.

Key words: acceleration of particles – shock waves – Sun: coronal mass ejections (CMEs) – Sun: particle emission

Online-only material: color figures

1. INTRODUCTION

Energetic particles are accelerated at shock waves in a wide variety of astrophysical settings. They are accelerated at planetary bow shocks, at the shocks formed at corotating interaction regions by high-speed solar-wind streams, and at the solar-wind termination shock at the outer boundary of the heliosphere. Galactic cosmic rays are accelerated at shock waves from supernovae. Yet the traveling interplanetary shock waves, driven out from the Sun by coronal mass ejections (CMEs), provide the greatest variety in shock conditions directly available for study, and we can measure the particle acceleration at these shocks, in situ, together with the local shock parameters (Gosling et al. 1981; Lee 1983, 2005; Jones & Ellison 1991; Desai et al. 2003, 2004; Tylka et al. 2005; Tylka & Lee 2006). Traveling interplanetary shocks are also of special interest since they are the observable remnants of the shock waves that are responsible for the large solar energetic-particle (SEP) events (Cliver et al. 1982; Gosling 1993; Kahler 1994; Reames 1995, 1999a; Kahler 2001; Tylka 2001; Ng et al. 2003; Tylka et al. 2005; Tylka & Lee 2006; Ng & Reames 2008; Sandroos & Vainio 2009; Rouillard et al. 2011).

Originally, the particles accelerated at interplanetary shocks were shown to come primarily from the solar wind (Gosling et al. 1981), evidence, in fact, that the energetic ions were indeed shock accelerated. However, in recent years there has been increasing recognition of the importance of other sources contributing to the "seed population" available for shock acceleration. Mason et al. (1999) first measured small but significant enhancements in abundances of ^{3}He/^{4}He in shock-accelerated particles and related the enhancement to the acceleration of remnant suprathermal ions from prior ^{3}He-rich impulsive flares which often have ^{3}He/^{4}He ∼ 1 in contrast with ^{3}He/^{4}He $\sim 5 \times 10^{-4}$ in the solar wind. Subsequently other abundances, such as Fe/O and the ionization states of Fe, were attributed to impulsive suprathermal ions in the seed population (Tylka et al. 2001; Desai et al. 2003, 2004). These suprathermal ions have the significant advantage of prior energization and they may be preferentially selected depending upon θ_{Bn}, the angle between the magnetic field, $\boldsymbol{B}$, and the shock normal, $\boldsymbol{n}$, since higher speeds may be required for the ions to overtake a quasi-perpendicular shock with $\theta_{\mathrm{Bn}} \sim 90^\circ$ (Tylka et al. 2005; Tylka & Lee 2006). It is now generally recognized that the seed population for a given shock may involve previously accelerated energetic ions from any source, including previous shocks (Desai et al. 2003, 2004).

Most of the recent studies of shock-accelerated particles and their seed populations involve abundances of elements and ions and not energy spectra. However, Desai et al. (2004) studied ion spectra and found that spectral indices were often independent of shock parameters, such as the shock compression ratio. These authors suggested that the shocks elevate the spectra of the seed population and they showed that the spectral indices of O and Fe do correlate with the spectra of the ambient upstream population. However, we may well ask what factors determine whether an observed spectral index derives from the shock compression ratio or from the upstream seed population. We should note that multi-spacecraft studies of local shocks find considerable spatial differences in the behavior of both the accelerated particles and the shock parameters (Neugebauer & Giacalone 2005; Koval & Szabo 2010).

Observational studies of shock acceleration often overlook the fact that there are many interplanetary shocks that do not seem to accelerate particles at all. In some sense these shocks are "too weak," but what determines whether the peak intensity is observable? To decide this we must compare the properties of shocks that *do not* significantly accelerate particles with those that do. In fact, we must look at particle acceleration in a randomly or independently selected sample of shock waves for which the shock parameters are measured. It so happens that there is a database of 285 shocks with complete analysis of the plasma data, measured on the *Wind* spacecraft, by J. Kasper (http://www.cfa.harvard.edu/shocks/wi_data/). This database is an extension of earlier work by Berdichevsky et al. (2000). In this paper, we use this shock database together with energetic-particle measurements to study the properties of shocks that do and do not accelerate particles. The energetic-particle data we use come from the Low Energy Matrix Telescope (LEMT) also on the *Wind* spacecraft (von Rosenvinge et al. 1995). Since element abundances have been emphasized in previous studies, for simplicity we confine our attention here to the energy spectra of the single element He in the ∼1–10 MeV amu^{-1} interval available from LEMT.

2. EXPECTED SHOCK SPECTRA

The re-acceleration of a power-law spectrum from a seed population may be treated as an example of the classical multiple-shock reacceleration problem (e.g., Axford 1981; Melrose & Pope 1993). Here, the equilibrium distribution function $f(p)$ of momentum p of accelerated particles downstream of the shock with compression ratio r is

$$f_a(p) = ap^{-a} \int_0^p dq\, q^{a-1}\phi(q), \tag{1}$$

where $a = 3r/(r - 1)$ and $\phi(p)$ is the injected distribution. If $\phi(p) = k\delta(p - p_0)$, then

$$f_a(p) = \frac{ak}{p_0}\left(\frac{p}{p_0}\right)^{-a} \quad \text{for } p > p_0, \quad f_a(p) = 0 \quad \text{for } p < p_0. \tag{2}$$

For simplicity, we neglect any adiabatic decompression of this first population that would reduce the overall intensity, but not change the spectral shape.

For acceleration of this population by a second shock with compression ratio r', we set $\phi(p) = f_a(p)$, and let $b = 3r'/(r' - 1)$. Integrating the power-law forms for $p > p_0$, we find

$$f_{a,b}(p) = \frac{kab}{p_0(b-a)}\left[\left(\frac{p}{p_0}\right)^{-a} - \left(\frac{p}{p_0}\right)^{-b}\right] \quad \text{for } a \neq b \tag{3}$$

and

$$f_{a,a}(p) = \frac{ka^2}{p_0}\left(\frac{p}{p_0}\right)^{-a} \ln\left(\frac{p}{p_0}\right) \quad \text{for } a = b. \tag{4}$$

However, there may also be acceleration from the solar wind at the second shock producing an additional contribution

$$f_b(p) = \frac{bk'}{p_0}\left(\frac{p}{p_0}\right)^{-b}, \tag{5}$$

which may or may not be significant, depending upon the values of k' and b. Finally, mapping to energy space, the intensity $j(E) = p^2 f(p)$.

From Equation (3), it is clear that the reaccelerated spectrum will be dominated by the stronger of the two shocks with the harder, flatter spectrum. The spectra of the first and second shocks appear symmetrically.

Power-law spectra are an equilibrium form that results from acceleration for an infinite time. While the acceleration time may be quite short in the solar corona (e.g., Ng & Reames 2008), it increases with the scattering coefficient and the particle energy and decreases inversely as the magnetic field, $\boldsymbol{B}$ (Ellison & Ramaty 1985). This effect results in a spectral break or "knee" that can be approximately (see Lee 2005) accommodated by modifying the power-law spectrum with a factor of $\exp(-E/E_0)$.

Combining these results, we have

$$j(E) \propto (E)^{-\gamma} \exp\left(E/E_0\right), \tag{6}$$

where, non-relativistically,

$$\gamma \approx \min\left[\gamma_{\rm bkg}, \frac{r_s + 2}{2(r_s - 1)}\right], \tag{7}$$

where $\gamma_{\rm bkg}$ is the energy spectral index of the upstream background seed population and r_s is the compression ratio of the second shock. Again, the hardest spectrum dominates the observed power law, but that spectrum is likely to roll downward at high energies.

Lee (2005) has considered spectral breaks in detail and in the exponential approximation (see Tylka & Lee 2006),

$$E_0 \propto (Q/A)\,(\sec\theta_{\rm Bn})^{2/(2\gamma-1)}, \tag{8}$$

where Q/A is the charge-to-mass ratio of the particle species considered.

3. EVENT SELECTION

To find the shock events with significant local particle acceleration we measured the average He intensity within 1 hr of the shock in eight LEMT energy intervals between 1 and 10 MeV amu^{-1} and compared it with the corresponding background intensity 8 hr upstream of the shock. To be selected, the intensity at the shock was required to be twice the background intensity in at least four of the eight energy intervals. From the 285 shocks in the Kasper list, we first eliminated eight that had data gaps or obscured data of energetic He, 18 reverse shocks, and one with no measured shock parameters, leaving 258 candidate shocks.

Applying our criteria to the energetic He at the 258 shocks resulted in 44 shocks with significant energetic-particle increases. In five of these events the He intensities continued to increase smoothly right past the shocks, these shocks having no apparent effect upon them. Eliminating these five shocks left us with 39 significant shock events. For a few of the shocks with sharply peaked He intensities, we decreased the averaging interval at the peak in order to obtain a more representative peak spectrum. Before considering the energetic-particle properties of the selected shock events, we compare the shock properties of the shocks that were, and were not, selected.

Figure 1 shows histograms of the distribution of the selected events within the overall distribution for three different shock parameters. A strong preference for high shock speed, V_s, is clearly seen for the selected events in the upper panel of the figure. Shocks with speeds <400 km s^{-1} rarely accelerate particles and the fraction with significant acceleration rises with V_s until nearly all shocks with V_s ∼ 1000 km s^{-1} accelerate particles. This preference for high shock speeds in local acceleration matches the findings of studies of particle acceleration in SEP events as a function of CME speed (e.g., Reames et al. 1997; Kahler 2001).

The middle panel in Figure 1 shows some tendency for greater particle acceleration in shocks with higher compression ratios. This probably occurs because the flatter spectra that may occur are more likely to produce measurable He intensities above

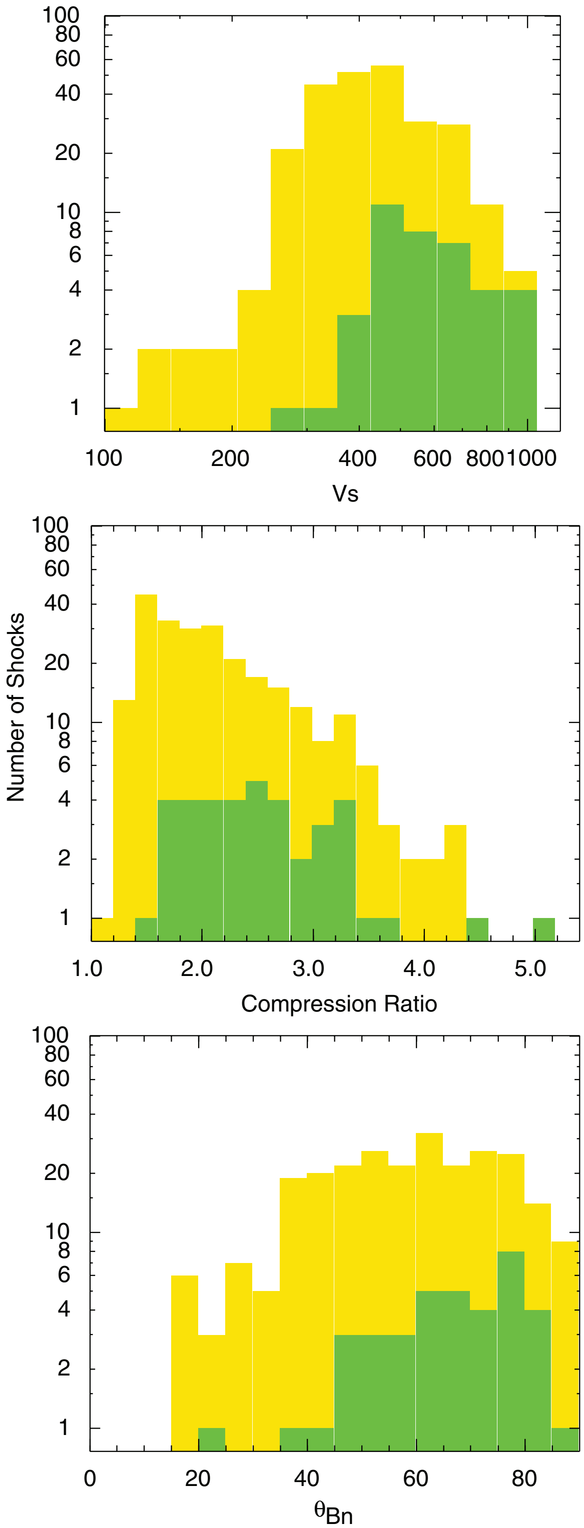

Figure 1. Histograms of the distribution of shocks with significant energetic-particle acceleration (green) are shown among the distribution for all shocks (yellow) as a function of shock speed (upper panel), shock compression ratio (middle panel), and shock normal angle (lower panel).

(A color version of this figure is available in the online journal.)

1 MeV amu^{-1}. The visibility of acceleration must surely depend upon the energy of observation and upon the sensitivity of the observing instrument or the level of the upstream background.

The distributions of θ_{Bn} are shown in the lower panel of Figure 1. If $\boldsymbol{B}$ is randomly directed relative to the shock normal, $\boldsymbol{n}$, the distribution of all events should increase like $\sin\theta_{\mathrm{Bn}}$. The observed distribution of all shocks in Figure 1 already has significant decreases from this expected distribution at the smallest and largest values of θ_{Bn}. However, the shocks with particle acceleration appear to have an additional reduction when $\theta_{\mathrm{Bn}} < 45°$. Overall, we find acceleration at 39 out of 258 shocks, or 15%; the corresponding rate for $\theta_{\mathrm{Bn}} \geqslant 45°$ is a slightly larger value of 18%. If we divide θ_{Bn} into three intervals, 0°–30°, 30°–60°, and 60°–90°, the probability of finding measurable acceleration in each interval is 6.2% ± 6.2%, 9.6% ± 2.9%, and 21.1% ± 4.1%, respectively. It is possible that quasi-perpendicular shocks are more likely to accelerate particles since shock drift may transfer a greater increment of energy each time a particle encounters the shock. This occurs because the $\sec\theta_{\mathrm{Bn}}$ factor in Equation (8) can extend the power-law spectrum to energies into our region of observation; spectra of quasi-parallel shocks break downward at much lower energies, i.e., below our energy of observation. However, it is also true that quasi-parallel shocks also have a slower decrease of intensity with distance from the shock and may be somewhat more likely to be rejected by our selection criteria.

4. SHOCKS WITH SIGNIFICANT ACCELERATION

4.1. Spectra

Shock properties[1] and He spectral indices are shown in Table 1 for the 39 shocks found to have significant particle acceleration. Errors on the shock parameters are derived from the standard deviation of eight methods of determining the parameters. For identification we have retained sequence numbers of the shocks from the original Kasper list. Unfortunately, for three of the shocks, shock 208 and the shock pair 224 and 225, LEMT is saturated right at the shock peaks so the intensities and spectra cannot be measured. For another shock pair, 133 and 134, the effects of the two shocks cannot be resolved. The observed and background spectral indices are least-squares fits to the eight-point energy spectra. The "observed" spectra are corrected for background before plotting or fitting.

For the shocks with measurable spectra, we compare the observed spectral indices with the background and calculated shock spectral indices in Figure 2. Certain shocks are identified by number in the figure for more detailed examination and discussion. Before we begin to discuss the shocks that are outliers in Figure 2, we show data for one shock that is typical of many where the spectral indices agree, shock 83.

Data for shock 83 are shown in Figure 3. The presence of the shock is clear in the plasma data as is the shock peak in the energetic-particle data. The fit to the background-corrected shock spectrum tends to emphasize the low energies because they are statistically more accurate. This reveals a spectral knee that begins to appear above about 4 MeV amu^{-1}. Note that if a knee had begun below ∼2 MeV amu^{-1}, we might have concluded that the observed spectrum was too steep to agree with either the shock or the upstream background spectra.

Next consider shock 51 shown in Figure 4. This is an example of shocks, such as 63 and 68, with observed spectra that are steeper than the calculated spectra and much steeper than the spectra of the upstream background. Perhaps spectral knees may explain why the observed spectra are steeper than the calculated shock index; however, the background in these events is extremely low. In fact, the background of $\sim 2 \times 10^{-5}$

[1] http://www.cfa.harvard.edu/shocks/wi_data/

Table 1
Properties of Shocks with Significant Particle Acceleration

Shock time (UT)	Shock Num.	V_shock (km s^{-1})	Shock Compression	θ_{Bn} (deg)	Calculated Index	Observed Index	Background Index
1997 May 15 0115	51	413 ± 48	2.17 ± 0.13	84 ± 4	3.8 ± 0.4	4.87 ± 0.13	1.83 ± 0.21
1997 Nov 22 0912	63	456 ± 41	2.54 ± 0.07	79 ± 10	3.5 ± 0.1	6.19 ± 0.10	3.15 ± 0.29
1997 Dec 30 0113	68	375 ± 34	2.03 ± 0.17	71 ± 9	4.0 ± 0.5	4.84 ± 0.42	0.03 ± 0.27
1998 Aug 6 0716	83	465 ± 13	1.92 ± 0.24	80 ± 3	4.1 ± 0.9	4.54 ± 0.25	4.78 ± 0.16
1998 Aug 26 0640	87	648 ± 115	2.88 ± 0.31	68 ± 20	3.3 ± 0.5	2.56 ± 0.35	1.97 ± 0.17
1998 Sep 24 2320	88	733 ± 104	2.17 ± 0.38	78 ± 7	3.8 ± 1.0	3.19 ± 0.20	2.76 ± 0.08
1999 Sep 22 1209	117	460 ± 46	2.64 ± 0.68	77 ± 9	3.4 ± 1.2	5.85 ± 0.19	4.42 ± 0.09
2000 Feb 11 2334	124	608 ± 99	3.27 ± 0.50	84 ± 8	3.2 ± 0.6	3.83 ± 0.21	3.71 ± 0.10
2000 Jun 23 1257	132	488 ± 38	2.56 ± 0.54	63 ± 13	3.5 ± 1.0	5.80 ± 0.18	4.60 ± 0.14
2000 Jul 13 0943	133	607 ± 71	2.44 ± 0.24	44 ± 14	3.5 ± 0.5	3.64 ± 0.12	2.99 ± 0.08
2000 Jul 13 0959	134	726 ± 120	1.83 ± 0.25	56 ± 16	4.3 ± 1.1		
2000 Jul 19 1530	135	615 ± 54	3.21 ± 0.29	54 ± 10	3.2 ± 0.3	2.89 ± 0.08	1.61 ± 0.15
2000 Jul 28 0638	139	476 ± 32	2.82 ± 0.74	54 ± 6	3.3 ± 1.1	1.11 ± 0.22	2.38 ± 0.09
2000 Aug 11 1849	141	564 ± 42	2.67 ± 0.58	76 ± 8	3.4 ± 1.0	3.26 ± 0.12	3.81 ± 0.15
2000 Oct 5 0328	146	525 ± 31	2.35 ± 0.25	77 ± 5	3.6 ± 0.6	5.07 ± 0.35	3.97 ± 0.30
2000 Oct 12 2233	147	520 ± 9	2.43 ± 0.24	71 ± 6	3.6 ± 0.5	4.18 ± 0.11	2.81 ± 0.08
2000 Nov 4 0225	151	429 ± 21	2.28 ± 0.21	68 ± 17	3.7 ± 0.5	3.19 ± 0.16	3.70 ± 0.20
2001 Apr 7 1756	178	552 ± 118	3.24 ± 0.33	78 ± 12	3.2 ± 0.4	3.44 ± 0.19	2.72 ± 0.08
2001 Apr 8 1120	179	646 ± 145	2.70 ± 0.42	61 ± 20	3.4 ± 0.7	4.03 ± 0.21	3.37 ± 0.14
2001 Apr 28 0500	185	900 ± 78	3.10 ± 1.36	47 ± 11	3.2 ± 1.7	4.50 ± 0.20	3.03 ± 0.18
2001 May 12 1003	187	566 ± 21	1.44 ± 0.03	65 ± 9	5.9 ± 0.4	3.21 ± 0.12	3.05 ± 0.21
2001 Sep 14 0159	207	472 ± 15	1.97 ± 0.24	59 ± 4	4.0 ± 0.8	3.13 ± 0.20	3.08 ± 0.12
2001 Sep 25 2017	208	534 ± 436	3.00 ± 2.06	68 ± 7	3.2 ± 2.8	sat	1.07 ± 0.28
2001 Nov 24 0454	224	637 ± 43	1.67 ± 0.33	48 ± 20	4.7 ± 2.0	sat	0.98 ± 0.18
2001 Nov 24 0551	225	1015 ± 20	5.12 ± 1.09	85 ± 5	2.9 ± 0.6	sat	0.98 ± 0.18
2002 Feb 17 0332	240	329 ± 13	2.63 ± 0.18	51 ± 8	3.4 ± 0.3	2.80 ± 0.25	3.21 ± 0.21
2002 Mar 18 1314	245	510 ± 186	2.29 ± 0.37	46 ± 14	3.7 ± 0.9	4.22 ± 0.22	4.09 ± 0.23
2002 Apr 17 1101	249	487 ± 76	2.45 ± 0.20	61 ± 11	3.5 ± 0.4	3.75 ± 0.11	3.21 ± 0.18
2002 Apr 19 0825	250	770 ± 46	3.23 ± 0.41	76 ± 4	3.2 ± 0.5	3.02 ± 0.14	3.24 ± 0.11
2002 May 23 1044	256	722 ± 22	1.72 ± 0.39	74 ± 4	4.6 ± 2.1	2.59 ± 0.30	2.08 ± 0.26
2002 Jul 17 1555	260	464 ± 40	3.14 ± 0.74	38 ± 8	3.2 ± 0.9	3.02 ± 0.33	2.27 ± 0.25
2002 Sep 3 1817	264	297 ± 89	4.46 ± 0.47	66 ± 17	2.9 ± 0.3	2.63 ± 0.16	2.82 ± 0.18
2002 Sep 7 1622	265	878 ± 24	1.73 ± 0.26	81 ± 8	4.6 ± 1.4	2.49 ± 0.27	1.93 ± 0.16
2003 May 29 1831	271	890 ± 41	2.03 ± 0.29	75 ± 4	4.0 ± 0.9	3.00 ± 0.15	2.44 ± 0.13
2003 May 30 1553	272	813 ± 63	3.39 ± 1.13	74 ± 5	3.1 ± 1.2	3.28 ± 0.18	3.15 ± 0.14
2003 Jun 18 0901	274	396 ± 124	1.79 ± 0.20	58 ± 26	4.4 ± 0.9	1.70 ± 0.22	1.82 ± 0.18
2004 Jul 26 2225	280	1012 ± 191	3.61 ± 0.79	63 ± 15	3.1 ± 0.8	2.07 ± 0.30	2.34 ± 0.18
2004 Aug 29 0909	281	482 ± 10	1.88 ± 0.22	24 ± 6	4.2 ± 0.9	1.94 ± 0.17	2.32 ± 0.56
2004 Nov 7 1759	282	742 ± 27	2.27 ± 0.34	60 ± 7	3.7 ± 0.8	3.85 ± 0.16	3.04 ± 0.19

particles (cm^2 sr s MeV amu^{-1})$^{-1}$ seen at higher energies in Figure 4 is determined by anomalous cosmic ray (ACR) He from the outer heliosphere (e.g., Reames 1999b). For shock 68 the entire background at all energies is from ACR He. The ACR spectrum, dominant at solar minimum, is present for all of these small events in 1997. In the weighted integral over the seed population in Equation (1), the solar-wind suprathermals appear to dominate the ACRs as they dominate the very flat background spectrum in shock 51. Incidentally, the accelerated abundances in these events indeed reflect solar-wind abundances (e.g., O/C ∼ 2) not ACR abundances (O/C ∼ 20).

The observed spectra of shocks 117 and 132 also appear to be steeper than expected from either the background spectrum or from the shock compression ratio, as shown in Figure 2. Observations for shock 117 are shown in Figure 5. The spectrum for shock 117 is seen to be rolling downward at high energies, a process that may have begun somewhat below the energy region we observe.

Figure 6 shows the observations for shock 135. This shock agrees with the calculated spectrum but is not affected by the flatter background spectrum. It is possible that background at energies below ∼1 MeV amu^{-1} is actually steeper than that part of the spectrum we can observe in the 1–10 MeV amu^{-1} region. Such differences in the seed population spectrum below the energy of observation may explain some of the scatter of the events about the diagonal in the lower panel of Figure 2.

Shock events above the diagonal in the upper panel of Figure 2 that fall near the diagonal in the lower panel, such as shocks 187 and 274, are exactly as expected from Equation (3) or Equation (8). These shocks have spectra that are dominated by the hard background spectrum at a weaker shock. Shock 139 is similar, but its spectrum is even harder than the background. Figure 7 shows that the plasma near shock 139 is quite complicated. The directions of $\boldsymbol{B}$ have been added to the figure to show that the shock may be traversing multiple flux tubes in that region. The observed spectrum at the shock is actually quite rounded and does not follow our simple description.

4.2. Intensities

Having selected the shock events, we can now explore the effect of the shock parameters on the observed intensities at the shock peak. In Figure 8, we show the dependence of the peak intensity, in the 1.65–2.00 MeV amu^{-1} energy interval, upon

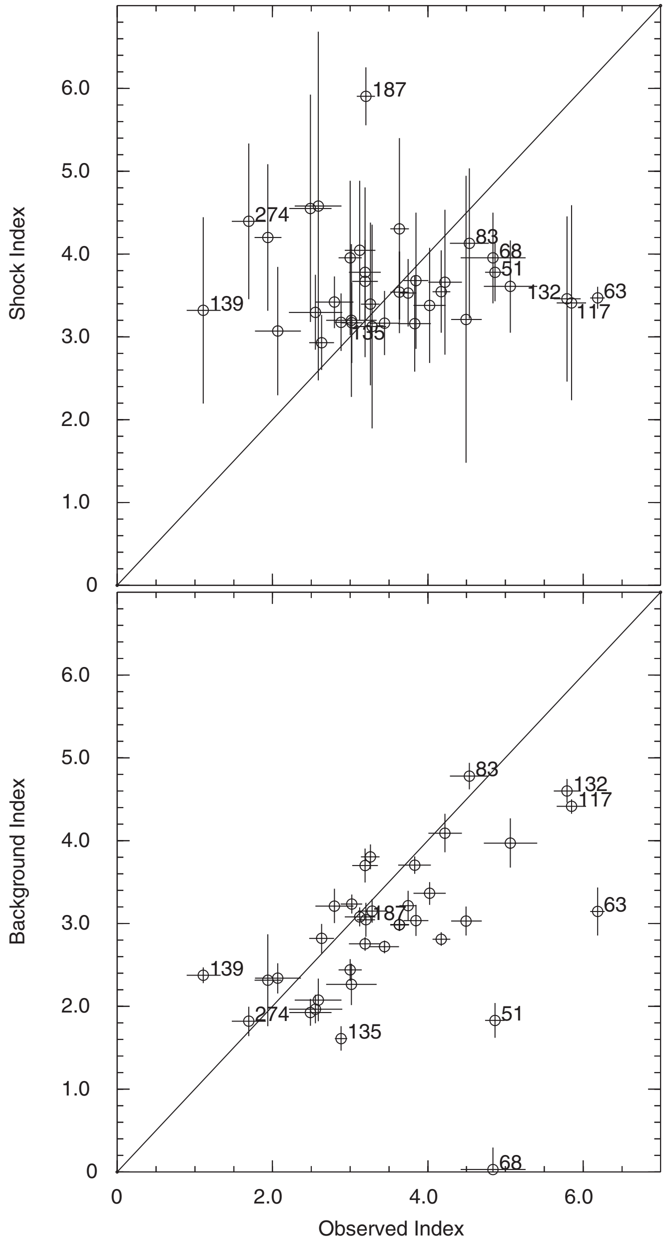

Figure 2. Comparison is shown of the calculated shock spectral index (upper panel) and the background spectral index (lower panel) as a function of the observed spectral index. Some shocks are identified by number in the figure for discussion in the text.

the shock speed, the compression ratio, and the shock-normal angle, θ_{Bn}. Weighted least-squares fit lines are shown for each of the three cases and the corresponding correlation coefficients are 0.808, 0.354, and 0.117 for the shock speed, the compression ratio, and θ_{Bn}, respectively. Thus, shock speed is a strong predictor of particle intensity in this local setting just as CME speed was found to be strongly correlated with particle intensity in large SEP events (e.g., Kahler 2001).

5. DISCUSSION

It may seem surprising that only 39 of 258 shocks at 1 AU, ~15%, have significant particle acceleration to 1–10 MeV amu^{-1}. The corresponding rate for $\theta_{Bn} \geqslant 45°$ is 36 out of 198 or ~18%. Thus, if there is a bias of our selection criteria against slowly rising quasi-parallel shocks, our

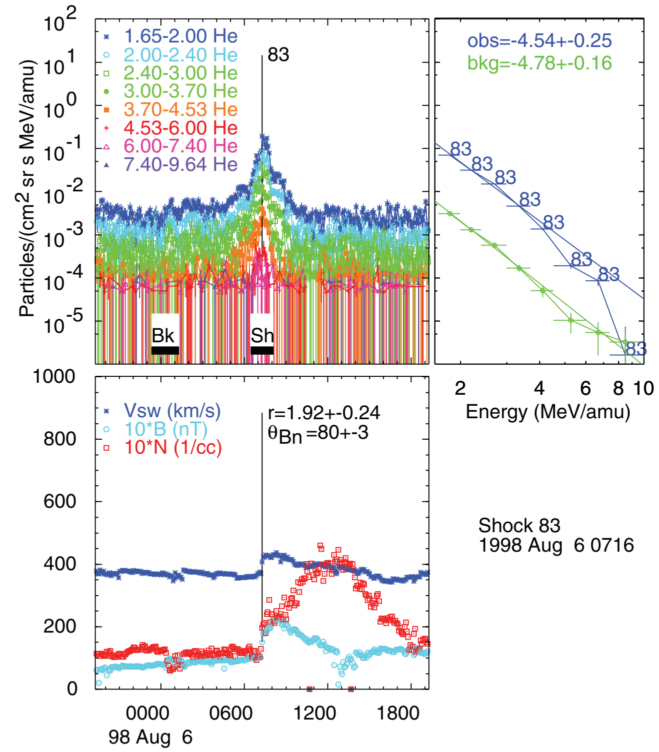

Figure 3. He time profiles of 5 minute averaged intensities in eight listed energy intervals are shown in the upper left panel for shock 83 while time variations in the solar-wind parameters, V_{SW}, B, and density, N, are shown in the panel below. Averaging intervals for the background and the shock are shown as "Bk" and "Sh", respectively, along the bottom of the upper left panel. The shock time is indicated by vertical lines and the shock compression ratio, r, and θ_{Bn} for shock 83 are listed. The upper right panel shows the background-corrected shock spectrum (blue) flagged by the shock number and the background spectrum (green) as well as least-squares fits to each spectrum.

(A color version of this figure is available in the online journal.)

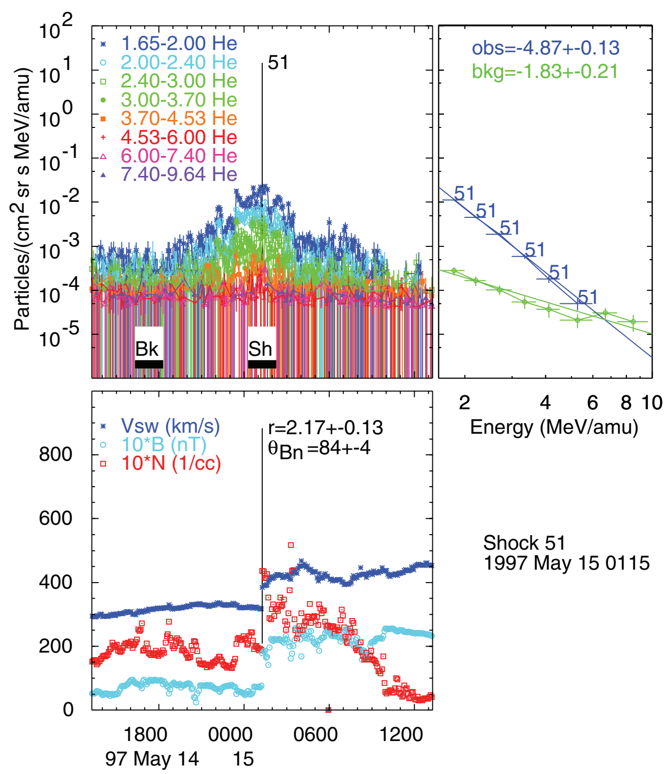

Figure 4. Data for shock 51 are shown as described in Figure 3.

(A color version of this figure is available in the online journal.)

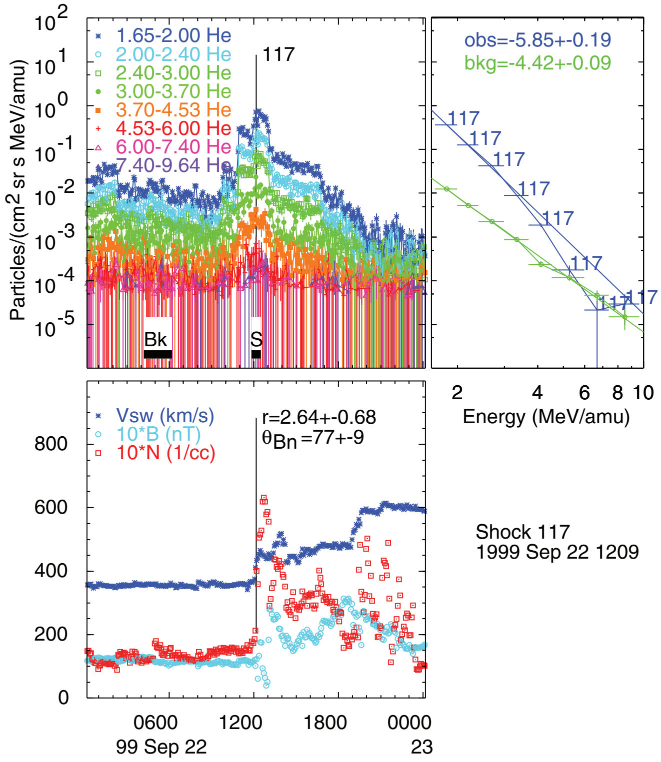

Figure 5. Data for shock 117 are shown as described in Figure 3.

(A color version of this figure is available in the online journal.)

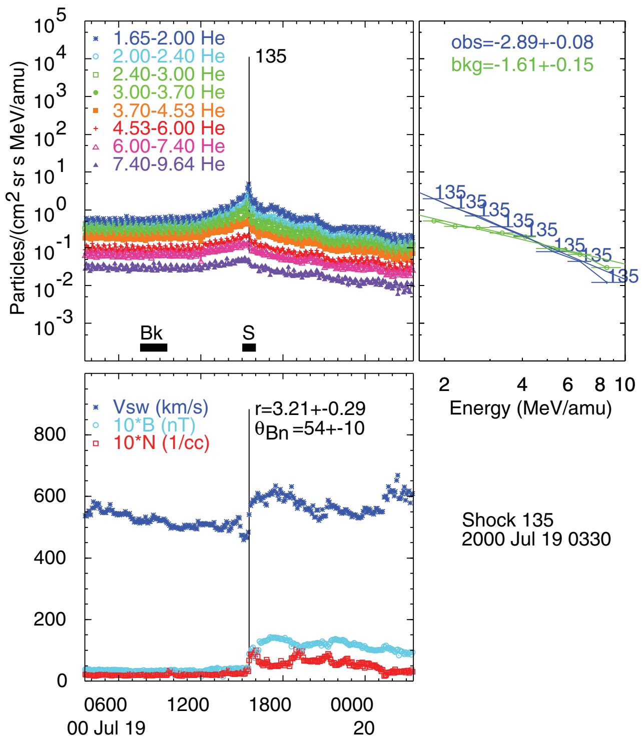

Figure 6. Data for shock 135 are shown as described in Figure 3.

(A color version of this figure is available in the online journal.)

success ratio would only increase minimally. Clearly, the most significant factor is the dependence of intensity on shock speed. However, an additional criterion may be that of energy-spectral shape. For over half of the 39 shocks, the intensity falls below background by 10 MeV amu^{-1}. This factor-of-two per decade would suggest that an instrument with equal sensitivity

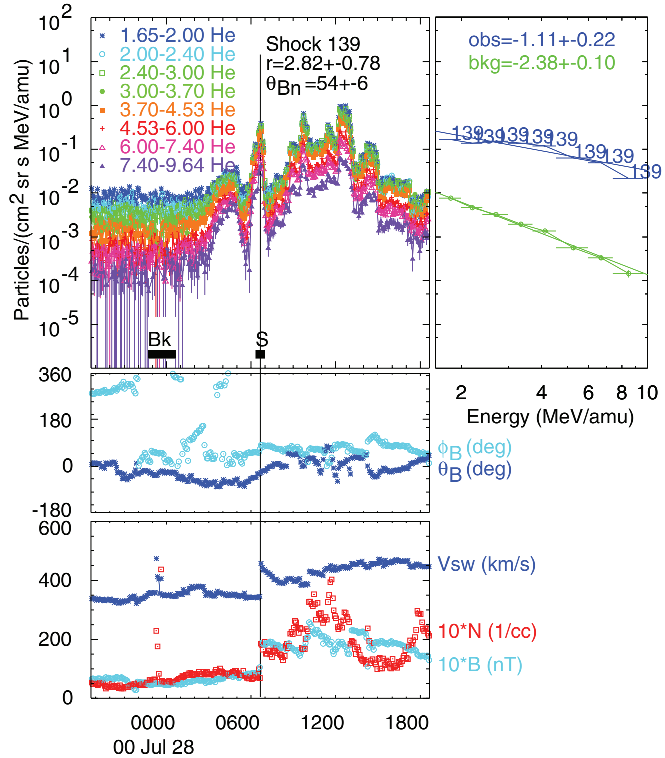

Figure 7. Data for shock 139 are shown as described in Figure 3 with an added middle panel showing the directions of ***B***.

(A color version of this figure is available in the online journal.)

(geometry factor), measuring down to $\sim$100 keV amu^{-1}, would find significant acceleration at nearly half of the 258 shocks. This means that the acceleration timescale has become long enough at 1 AU for spectral knees, E_0, to develop below 1 MeV amu^{-1} for He in many shocks, especially quasi-parallel shocks. The presence of a knee below $\sim$1 MeV amu^{-1} also explains why shocks 51 and 63, for example, have spectra that are steeper than expected.

Particle intensities are seen to depend strongly on V_s which is also related to the Alfvén Mach number $M_A = V_s/V_A$ where V_A is the Alfvén speed, which is typically $\sim$40 km s^{-1} near Earth. Thus shocks with speeds $>$400 km s^{-1}, required for observable acceleration, exceed Mach 10. The rate of plasma flow into the shock, ρV_s, hence the particle injection, also depends upon the shock speed. In addition, since the shock speed is approximately the CME speed, for a driven shock, the maximum energy available for particle acceleration by the shock may be $\sim m_{CME} {V_s}^2$. Thus, a strong dependence of accelerated particle intensity on shock speed is not surprising, but the explicit dependence is elusive.

For many cases the background spectral index is as hard as, or harder than, that calculated from the shock compression ratio. The shocks at 1 AU have been traveling for several days and the "background" consists of ions accelerated by the same shock at an earlier time when it was stronger. Unfortunately, we are unable to completely distinguish the seed population from the accelerated ions, not only because the seed spectrum extends to lower energies that we cannot observe. If we had chosen the background period 2 or 3 days earlier, before the shock left the Sun, solar rotation would have insured that we were selecting our seed population from magnetic flux tubes at solar longitudes of $\sim$26°–39° to the west of those of the accelerated ions. We believe that the best estimate of the seed population for local

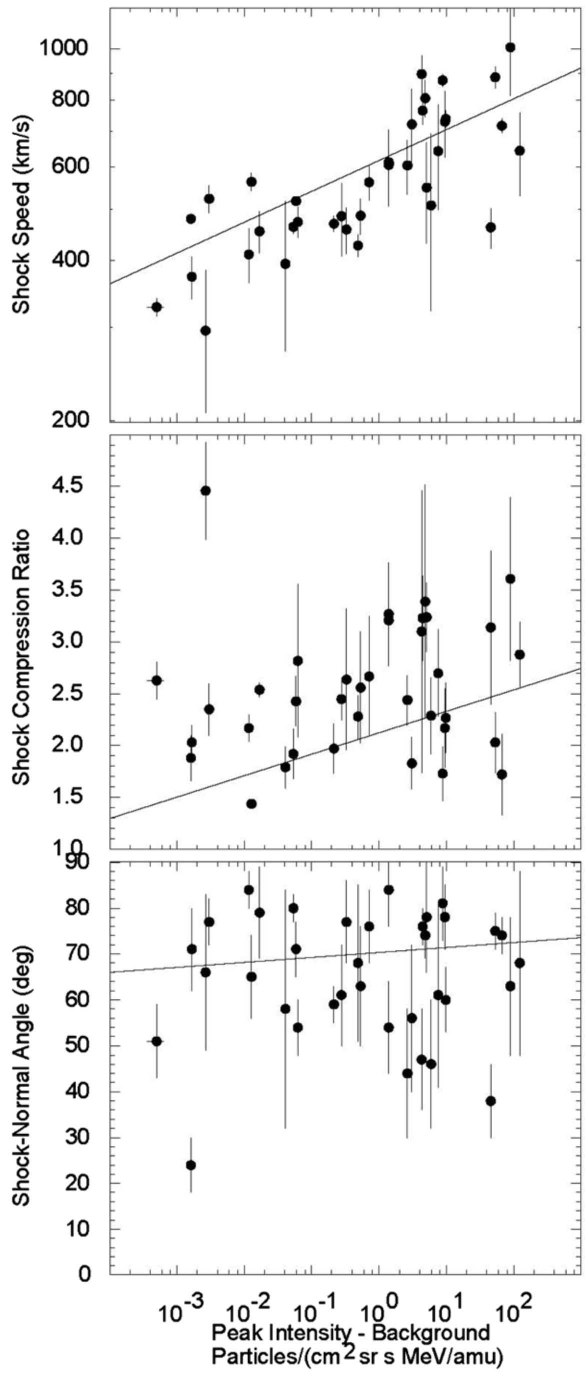

Figure 8. Background-corrected peak intensity at 1.65–2.00 MeV amu^{-1} is shown vs. shock speed, shock compression ratio, and θ_{Bn} for each shock, with weighted least-squares fit lines shown for each parameter.

acceleration was the ions nearby. Choosing a time period of 12 or 16 hr upstream of the shock made little difference in the spectra for most shocks, but for some, this "background" period occurred during an unrelated earlier event. We did not want to introduce a new selection criterion to reject these contaminated shocks nor did we want to abandon the objectivity of a fixed separation between the shock and the upstream background periods.

It has been called to our attention that a few shocks, e.g., 2001 November 6, are missing from the Kasper database, suggesting a possible selection bias against strong shocks. However, the shocks 208, 224, and 225 in Table 1 are sufficiently strong to accelerate intensities that saturate the LEMT detector, an extremely rare occurrence in itself that has happened only half a dozen times in 18 years. In any case, the loss of a few large events is unlikely to affect the statistics of our determination of the dependence of particle properties on shock parameters. On the contrary, our emphasis should really focus on the smallest events and the physical processes at the boundary distinguishing shocks that barely accelerate particles from those that fail to do so.

While we have not measured element abundances, the theory does suggest the origin of some abundance variations seen by other authors (e.g., Desai et al. 2003, 2004). The spectrum of each accelerated species is derived from a weighted integral over the spectrum of its seed population as in Equation (1). Thus, different accelerated species may be dominated by different energy regions of the seed population, resulting in accelerated abundances that vary with energy and differ from abundances at any particular energy of the seed population. Thus, abundance variations can arise even without recourse to the species dependence of E_0 (Tylka et al. 2001; Tylka & Lee 2006) or its systematic dependence on θ_{Bn} (e.g., Lee 2005; Tylka & Lee 2006) that have been considered.

Finally, we note that Zank et al. (2006) have suggested that "higher proton energies are achieved at quasi-parallel rather than highly perpendicular interplanetary shocks within 1 AU." The observations in this paper do not support that suggestion.

6. CONCLUSIONS

We have examined all 258 forward shocks in the Kasper database of shock measurements from the *Wind* spacecraft in an effort to find significant acceleration of He ions to the 1–10 MeV amu^{-1} interval using a well-defined set of selection criteria. The most important determinant of selection was the shock speed, followed by the shock compression ratio. Quasi-perpendicular shocks were also favored, perhaps partly because of our selection criteria, but more likely because of the dependence of the *e*-folding or knee energy on θ_{Bn}. The importance of shock speed in the selection is undoubtedly because the peak intensity at the shock depends strongly upon shock speed as is seen in Figure 8.

The observed spectral index for most of the selected shocks agreed with that calculated from the shock compression ratio or with that of the upstream background, whichever was flatter, as expected from diffusive shock theory. Spectra of typical shocks that seemed to depart from theory were exhibited and discussed individually.

Exponential rollovers or knees were often clearly seen despite the limited energy interval studied. Similar knees below $\sim$1 MeV amu^{-1} probably explain some of those few shocks with unexpectedly steep observed spectra. Low-energy knees undoubtedly also affect many shocks, especially quasi-parallel shocks, where locally accelerated ions were not observed at all. Together, low-energy knees, steep spectra (i.e., weak shocks), and low shock speeds probably explain those shocks with no apparent acceleration.

This work was funded in part by NASA grant NNX08AQ02G.

REFERENCES

Axford, W. I. 1981, in Proc. 17th Int. Cosmic Ray Conf. 12 (Gif-sur-Yvette: CEA), 155

Berdichevsky, D. B., Szabo, A., Lepping, R. P., Viñas, A. F., & Mariana, F. 2000, J. Geophys. Res., 105, 27289

Cliver, E. W., Kahler, S. W., Shea, M. A., & Smart, D. F. 1982, ApJ, 260, 362
Desai, M. I., Mason, G. M., Dwyer, J. R., et al. 2003, ApJ, 588, 1149
Desai, M. I., Mason, G. M., Wiedenbeck, M. E., et al. 2004, ApJ, 661, 1156
Ellison, D., & Ramaty, R. 1985, ApJ, 298, 400
Gosling, J. T. 1993, J. Geophys. Res., 98, 18937
Gosling, J. T., Asbridge, J. R., Bame, S. J., et al. 1981, J. Geophys. Res., 86, 547
Jones, F. C., & Ellison, D. E. 1991, Space Sci. Rev., 58, 259
Kahler, S. W. 1994, ApJ, 428, 837
Kahler, S. W. 2001, J. Geophys. Res., 106, 20947
Koval, A., & Szabo, A. 2010, J. Geophys. Res., 115, A12105
Lee, M. A. 1983, J. Geophys. Res., 88, 6109
Lee, M. A. 2005, ApJS, 158, 38
Mason, G. M., Mazur, J. E., & Dwyer, J. R. 1999, ApJ, 525, L133
Melrose, D. B., & Pope, M. H. 1993, PASA, 10, 222
Neugebauer, M., & Giacalone, J. 2005, J. Geophys. Res., 110, A12106
Ng, C. K., & Reames, D. V. 2008, ApJ, 686, L123
Ng, C. K., Reames, D. V., & Tylka, A. J. 2003, ApJ, 591, 461
Reames, D. V. 1995, Rev. Geophys., 33, 585
Reames, D. V. 1999a, Space Sci. Rev., 90, 413
Reames, D. V. 1999b, ApJ, 518, 473
Reames, D. V., Kahler, S. W., & Ng, C. K. 1997, ApJ, 491, 414
Rouillard, A. C., Odstřcil, D., Sheeley, N. R., et al. 2011, ApJ, 735, 7
Sandroos, A., & Vainio, R. 2009, A&A, 507, L21
Tylka, A. J. 2001, J. Geophys Res., 106, 25333
Tylka, A. J., Cohen, C. M. S., Deitrich, W. F., et al. 2001, ApJ, 558, L59
Tylka, A. J., Cohen, C. M. S., Dietrich, W. F., et al. 2005, ApJ, 625, 474
Tylka, A. J., & Lee, M. A. 2006, ApJ, 646, 1319
von Rosenvinge, T. T., Barbier, L. M., Karsch, J., et al. 1995, Space Sci. Rev., 71, 155
Zank, G. P., Li, G., Florinski, V., et al. 2006, J. Geophys. Res., 111, A06108